Here I_0 is load current when there are no baffles. When the potential difference is specified, $I_0 = 2a/h(1-\phi_0)$, and when the load resistance R is given, $I_0 = 2a/(h+aR)$. Since in Eq. (16) the coefficient of $(1-\alpha)$ is positive, this means that the placing of baffles increases the net current.

In our calculations, the velocity distribution $u_0(x)$ was expressed as

$$u_0(x) = m\frac{\cosh m - \cosh(mxh/a)}{m\cosh m - \sinh m}$$

and when parameter m goes from zero to infinity the distribution varies from the parabolic (Poiseuille distribution) to the homogeneous.

Figure 3 depicts calculated curves of current I as a function of size α of the baffles. At $\alpha = 0$ (the channel is completely blocked by the baffles, Fig. 2) $I(\alpha=0)=0$, however, the decrease in the current to zero with increase of baffle size is very slow. Since $I(\alpha=0)=0$ and Eq. (16) is fulfilled at $\alpha \simeq 1$, curves $I(\alpha)$ have maxima. However, calculations show that, as m is increased, whereupon the velocity distribution becomes fuller, which corresponds to the case of a real MHD generator, the curve of $I(\alpha)$ becomes flat without a sharply expressed peak. The latter fact allows the conclusion that in order to increase the net current it suffices to place small baffles. This is important, since it can be expected that the additional friction produced by placing these rather small baffles will not be so high as to significantly lessen the benefit of suppression of current flow reversal.

Acknowledgment

This work was supported in part by the Office of Naval Research, U.S.A., under grant N00014-77-G-0034. The authors wish to thank H. Branover for discussion of their work and D. Michelson for performing the computations.

References

[1] Sutton, G. W., "Design Considerations of a Magnetohydrodynamic Electrical Power Generator," *Vistas Astronautics*, Vol. 3, SPE, New York, 1960, pp. 53-64.

[2] Carrier, G., Krook, M., and Pearson, C., *Functions of a Complex Variable*, McGraw-Hill, N.Y., 1966.

[3] Keldysh, M. V. and Sedov, L. I., "Effective Solution of some Boundary Value Problems for Harmonic Functions," *Doklady Akademii Nauk SSSR*, Vol. 16, No. 1, 1937, pp. 7-10

Finite Deformation of Anisotropic Plastic Rotating Disks

William W. Feng*
University of California, Livermore, Calif.

Introduction

MOST rolled sheet metals exhibit variations of yield stress and stress-strain relations with orientation, while the sheet remains approximately isotropic in its plane. This phenomenon was verified experimentally by Lilet and Wybo.[1] Constitutive equations for anisotropic plastic materials that harden according to a power law were developed by Hill.[2] The anisotropic property of the material is measured by a strain-ratio parameter that is defined on the basis of a uniaxial test as the ratio of the transverse plastic strain in the plane of the sheet to the plastic strain through the thickness. The strain hardening property is characterized by a constant that is the exponent of a power law relating the effective stress and strain. These constitutive equations and their influence on drawability of the degree of anisotropy and on the strain hardening characteristics have been studied by Budiansky and Wang.[3] Yang[4] has analyzed the stress concentration of circular sheets with imperfections using the same equations. In this Note, these equations are used to solve the nonlinear problem of rotating disks. The rotating disks exhibit anisotropic properties in planes other than their own. The material properties in the rotating plane are assumed to be isotropic; therefore, the axisymmetric rotating disk before deformation remains axisymmetric after deformation.

In the formulation and numerical calculations, large strains and finite deformations are considered. The formulation is similar to that used by Feng[5] in studying hyperelastic rubber disks under various loadings. The strains in the radial and circumferential directions are used as two dependent variables. The governing equations are reduced to two coupled first-order ordinary differential equations with explicit derivatives, and further reduced with the boundary conditions, to dimensionless forms. The equations with their appropriate boundary conditions can be solved by any numerical integration method. We have also introduced an efficient numerical method that eliminates the iteration scheme to satisfy the governing equations and the boundary conditions. Stress and strain distributions for a solid rotating disk are also included.

The results obtained in this paper can be applied directly to the study of the mechanics of flywheels. The formulation and numerical method can be extended to the whole class of axisymmetric plane-stress and axisymmetric membrane problems.

Formulation

A rotating disk of anisotropic plastic material before and after deformation is shown in Fig. 1. A point p on the undeformed disk can be described by the undeformed polar coordinates (r,θ). Point p is deformed to point P and can be described by the deformed polar coordinates (R,Θ). For the axisymmetric problems, $\Theta = \theta$ and R is an unknown function of r. In the analysis, the disk is assumed to be thin and the plane-stress problem leads to a good approximation.

The strain in the radial, tangential, and normal directions are defined respectively as

$$\epsilon_r = \ell n\,(dR/dr) \quad \epsilon_\theta = \ell n\,(R/r) \quad \epsilon_z = \ell n\,(H/h) \qquad (1)$$

where H is the thickness of the deformed disk and h (a constant in this analysis) is the thickness of the undeformed disk.

The total stress-strain relations derived from Hill's[2] incremental relation for anisotropic plasticity are

$$\epsilon_r = \frac{\epsilon}{\sigma}\left[\sigma_r - \frac{\Gamma}{1+\Gamma}\sigma_\theta\right]$$

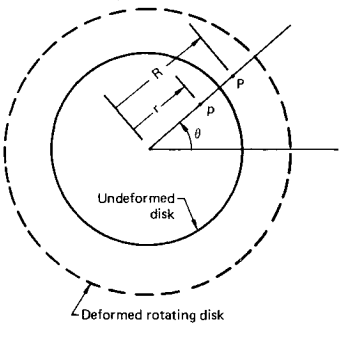

Fig. 1 Coordinates for a rotating disk.

Received Jan. 3, 1978. This paper is declared a work of the U.S. Government and therefore is in the public domain.

Index categories: Materials, Properties of; Analytical and Numerical Methods.

*Mechanical Engineer, Lawrence Livermore Laboratory.

and

$$\epsilon_\theta = \frac{\epsilon}{\sigma}\left[\sigma_\theta - \frac{\Gamma}{1+\Gamma}\sigma_r\right] \tag{2}$$

where σ is the effective stress and ϵ is the effective strain. The effective stress is related to the radial stress σ_r and the circumference stress σ_θ by

$$\sigma = \left(\sigma_r^2 + \sigma_\theta^2 - \frac{2\Gamma}{1+\Gamma}\sigma_r\sigma_\theta\right)^{1/2} \tag{3}$$

with a similar expression for the effective strain. The relation between the effective stress and the effective strain is

$$\sigma = k\epsilon^n \tag{4}$$

The material properties are completely defined by using Eqs. (2-4) and three constants Γ,k, and n. The anisotropic property of the disk is measured with the parameter Γ and the strain hardening property is measured with the parameter n.

The deformed thickness is related to the other physical quantities through the compressibility condition. We consider the incompressible material as

$$\epsilon_r + \epsilon_\theta + \epsilon_z = 0 \tag{5}$$

and

$$H = he^{-(\epsilon_r + \gamma_\theta)} \tag{6}$$

The equilibrium equations are satisfied automatically in the tangential and normal directions to the disk. The stresses must satisfy the equilibrium equation in the radial direction as

$$\frac{\mathrm{d}H\sigma_r}{\mathrm{d}R} + \frac{H}{R}(\sigma_r - \sigma_\theta) + H\rho R\omega^2 = 0 \tag{7}$$

where ρ and ω are the density and the angular velocity of the rotating disk.

In terms of the undeformed coordinate r, Eq. (7) reduces to

$$\frac{\mathrm{d}H\sigma_r}{\mathrm{d}r} + \frac{R'}{R}H(\sigma_r - \sigma_\theta) + \rho HRR'\omega^2 = 0 \tag{8}$$

where the prime denotes the differentiation with respect to r.

With Eqs. (2) and (6), the equilibrium Eq. (8) can be written in terms of the strains, and

$$G_r' = \frac{1}{F}\left\{\left[(n-1)\left(\epsilon_r + \frac{\Gamma}{1+\Gamma}\epsilon_\theta\right)\left(\epsilon_\theta + \frac{\Gamma}{1+\Gamma}\epsilon_r\right)\frac{1}{\epsilon} + \frac{\Gamma}{1+\Gamma}\epsilon - \epsilon\left(\epsilon_r + \frac{\Gamma}{1+\Gamma}\epsilon_\theta\right)\right]\epsilon_\theta' + \frac{1}{(1+\Gamma)r}e^{(\epsilon_r-\epsilon_\theta)}(\epsilon_r - \epsilon_\theta) + \frac{1+2\Gamma}{k(1+\Gamma)^2}\epsilon^{2-n}e^{(\epsilon_r+\epsilon_\theta)}\rho r\omega^2\right\} \tag{9}$$

where

$$F = (n-1)\left(\epsilon_r + \frac{\Gamma}{1+\Gamma}\epsilon_\theta\right)^2\frac{1}{\epsilon} + \epsilon - \epsilon\left(\epsilon_r + \frac{\Gamma}{1+\Gamma}\epsilon_\theta\right)$$

The companion equation obtained from the strain definition in Eq. (1) is

$$\epsilon_\theta' = [e^{(\epsilon_r-\epsilon_\theta)} - 1]/r \tag{10}$$

Equations (9) and (10), two coupled first-order ordinary differential equations, can be solved numerically. To improve further the numerical calculation, the following nondimensional quantities are introduced:

$$S = r/a, \qquad \Omega = \rho a^2\omega^2/k \tag{11}$$

where a is the radius of the undeformed disk. Equation (9) reduces to

$$\dot{\epsilon}_r = \frac{1}{SF}\left\{\left[(n-1)\left(\epsilon_r + \frac{\Gamma}{1+\Gamma}\epsilon_\theta\right)\left(\epsilon_\theta + \frac{\Gamma}{1+\Gamma}\epsilon_r\right)\frac{1}{\epsilon} + \frac{\Gamma}{1+\Gamma}\epsilon - \epsilon\left(\epsilon_r + \frac{\Gamma}{1+\Gamma}\epsilon_\theta\right)\right][e^{(\epsilon_r-\epsilon_\theta)} - 1] + \frac{1}{(1+\Gamma)}e^{(\epsilon_r-\epsilon_\theta)}\epsilon(\epsilon_r - \epsilon_\theta) + \frac{1+2\Gamma}{(1+\Gamma)^2}\epsilon^{2-n}e^{(\epsilon_r+\epsilon_\theta)}S^2\Omega\right\} \tag{12}$$

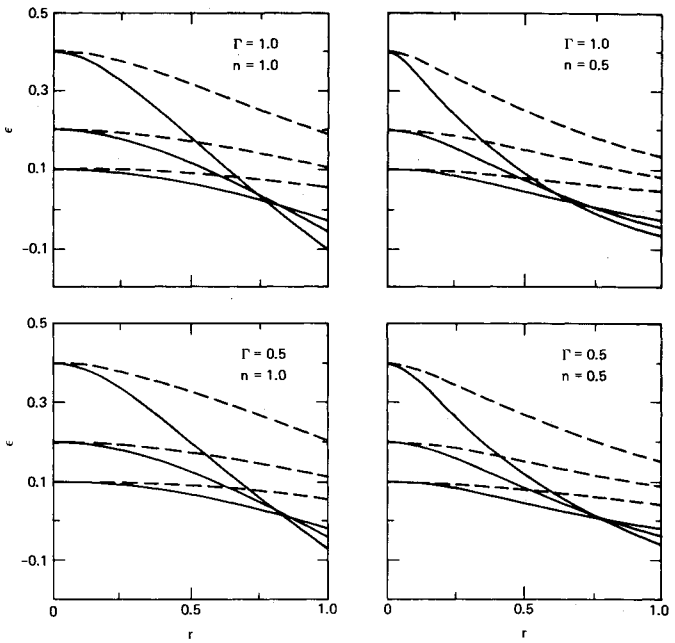

Fig. 2 Strain distribution for a rotating disk (solid lines denote ϵ_r, dashed lines ϵ_θ).

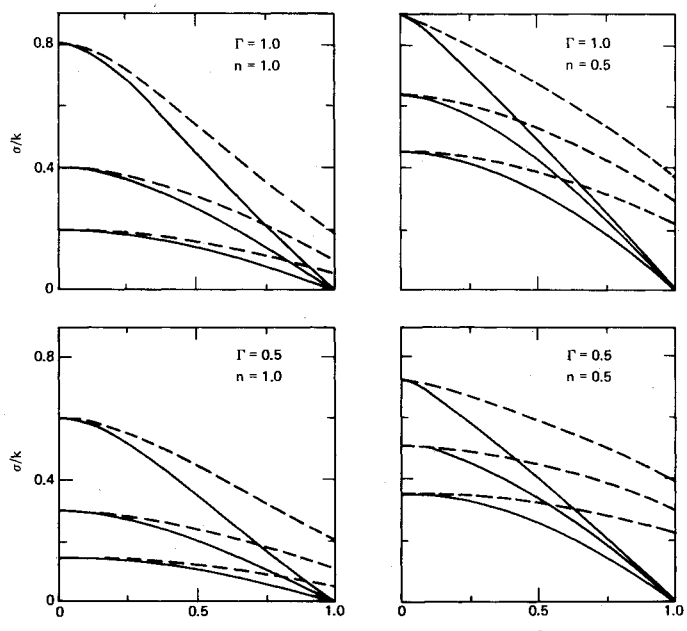

Fig. 3 Stress distribution for a rotating disk (solid lines denote σ_r, dashed lines σ_θ).

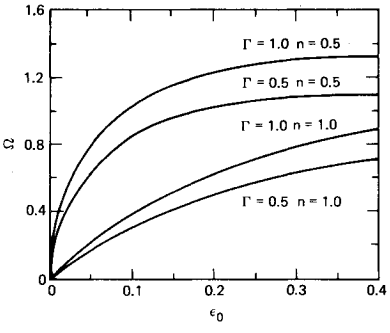

Fig. 4 Curves of Ω vs ϵ_0 for rotating disks.

and the companion Eq. (10) reduces to

$$\dot{\epsilon}_\theta = \{e^{(\epsilon_r - \epsilon_\theta)} - 1\}/S \tag{13}$$

where dots denote the differential with respect to the nondimensional quantity S, with F in Eq. (9) remaining unchanged. Equations (12) and (13) are similar to Eqs. (9) and (10); however, Eqs. (12) and (13) remain unchanged when the quantity S is multiplied by a scalar ξ and Ω is divided by ξ^2. This method eliminates the one-dimensional search technique for finding the solution numerically and will be explained in detail in the numerical calculation section.

The boundary conditions for a solid rotating disk are

$$S=0 \qquad \epsilon_r = \epsilon_\theta$$

$$S=1 \qquad \sigma_r = 0$$

or

$$\epsilon_r = -\frac{\Gamma}{1+\mathrm{E}}\epsilon_\theta \tag{14}$$

With these two boundary conditions and the governing Eqs. (12) and (13), the unknown functions for ϵ_θ and ϵ_r are determined.

Numerical Calculations

The boundary-value problem is changed into an initial-value problem by setting $\epsilon_r = \epsilon_\theta = \epsilon_0$ at $S=0$, providing two initial conditions for two first-order ordinary differential equations (12) and (13). The fourth-order Runge-Kutta method is used for the numerical integration, with an arbitrary value of Ω assigned. The solution can be obtained by increasing S until the second boundary condition is satisfied. It is not probable that the final $S(S_F)$ will have a value of 1 because ϵ_0 and Ω are not likely to have exact or consistent values. However, Eqs. (12) and (13) remain unchanged if S is multiplied by ξ and Ω is divided by ξ^2. If $\xi = 1/S_F$, then $\Omega_f = \Omega S_F^2$ is the exact solution that satisfies the differential Eqs. (12) and (13) and the boundary conditions in Eq. (14) for $\epsilon_r = \epsilon_\theta = \epsilon_0$ at $S=0$. Hence, the iteration procedures for adjusting Ω to satisfy the second boundary condition in Eq. (14) is eliminated.

Results

The governing differential equations with the boundary conditions and the numerical method previously discussed are programmed on a CDC 7600 computer, taking only a fraction of a second to obtain the solution for each case. The solution can also be obtained by using a programmable desk calculator. The results are presented in Figs. 2-4 where several ϵ_0's are assigned for various values of Γ and n. Curves of the strains ϵ_r and ϵ_θ vs r are shown in Fig. 2. After ϵ_r and ϵ_θ are determined, the stresses σ_r and σ_θ can be calculated from the conjugates of Eqs. (2). The deformed shape of the rotating disk can be obtained by determining R and

$$R = re^{\epsilon_\theta} \tag{15}$$

Once ϵ_r and ϵ_θ are determined, all other physical quantities are determined thereafter. Curves of the dimensionless stress σ_r/k and σ_θ/k vs r are presented in Fig. 3. Curves of Ω vs ϵ_0 are presented in Fig. 4. The foregoing results show that the stresses and strains are sensitive to the value Γ and n.

Discussion

The analysis presented in this paper can be applied directly to the study of flywheel mechanics. The governing equations are applicable to disks with a rigid inclusion and those with a hole. The boundary conditions for a disk with a concentric rigid inclusion are

$$S=r_c \qquad \epsilon_\theta = 0$$

$$S=1 \qquad \sigma_r = 0$$

or

$$\epsilon_r = -\frac{\Gamma}{1+\Gamma}\epsilon_\theta \tag{16}$$

where r_c is the dimensionless radius of the rigid inclusion. The dimensional radius is ar_c. The boundary conditions for a disk with a concentric hole are

$$S=r_h \qquad \sigma_r = 0$$

or

$$\epsilon_r = -\frac{\Gamma}{1+\Gamma}\epsilon_\theta$$

$$S=1 \qquad \sigma_r = 0$$

or

$$\epsilon_r = -\frac{\Gamma}{1+\Gamma}\epsilon_\theta \tag{17}$$

where r_h is the dimensionless radius of the hole before deformation and the dimensional value is ar_h. The mixed boundary-value problems presented in this paper have been converted into displacement boundary-value problems.

The material nonlinearity introduced through the stress-strain relation and the geometrical nonlinearity introduced by the occuring finite deformation, coupled with the complex analysis, indicates that numerical evaluation of the solution is mandatory. When $\Gamma = 1.0$ and $n = 1.0$, the material is isotropic and linear; however, the Ω vs ϵ_0 curve indicates nonlinearity as a result of the finite deformation formulation. Because Ω increases when Γ increases, for a given value ϵ_0 (Fig. 4), deformation can be minimized by choosing the proper value of Γ.

Acknowledgment

This work was performed under the auspices of the Department of Energy, under contract No. W-7405-Eng-48.

References

[1] Lilet, L. and Wybo, M., "The Effect of Plastic Anisotropy and Rate of Work-Hardening in Deep Drawing," *Sheet Metal Industries*, Vol. 41, 1964.

[2] Hill, R., *The Mathematical Theory of Plasticity*, Oxford University Press, 1950, Chap. 12.

[3] Budiansky, B. and Wang, N. M., "On the Swift Cup Test," *Journal of Mechanics and Physics of Solids*, Vol. 14, 1966, pp. 357-374.

[4] Yang, W. H., "Axisymmetric Plane Stress Problems in Anisotropic Plasticity," *Journal of Applied Mechanics*, Vol. 36, 1969, pp. 7-14.

[5] Feng, W. W., "On Rubber Disks Under Rotating or Axisymmetric Stretching," *International Journal of Nonlinear Mechanics*, Vol. 8, 1973, pp. 539-550.